Iraqi Journal of Physics, 2022 *Vol.20, No. 3, PP.86-97*

DOI: 10.30723/ijp.v20i3.1006

P-ISSN: 2070-4003
E-ISSN: 2664-5548

X-Ray Emission Spectroscopy Analysis for Near-Asteroid Belt of Atmospheric of the Comets

Rasha S. Najm[1a]*, Salman Z. Khalaf[1b], Khaleel I. Abood[1c]
[1]*Department of Astronomy and Space, College of Science, University of Baghdad, Baghdad, Iraq*
[b]E-mail: salman.zkhalaf@yahoo.com, [c]E-mail: khalel.Abod@yahoo.com
[a*]Corresponding author: rashasuhail8@gmail.com

Abstract

According to Chandra Survey Observatory Near-Asteroid Belt Comets, the solar wind's contact with the comet produces a variety of spectral characteristics. The study of X-ray spectra produced by charge exchange is presented here. The spectrum of a comet can reveal a lot about its composition. This study has concentrated on the elemental abundance in six different comets, including 17P/Holmes, C/1999T1, C/2013A1, 9p/Temple1, and 103p/Hartley2 (NEAT). Numerous aspects of the comet's dynamics allow it to behave in a unique manner as it gets closer to the Near-Asteroid Belt. These characteristics are being examined, and some studies are still ongoing. The computations allow us to observe, for instance, how the composition of a comet's upper atmosphere affects how much gas it produces. For several comet morphologies, both linear and nonlinear, bow shock, contact surface, and stagnation point are investigated in relation to gas production rate. Our results shed light on the complex interactions between cometary ions and the solar wind. An increase in gas production rate was shown to be significantly correlated with sharp drops in average molecular weight.

Article Info.

Keywords:
Abundance, energy, number density, bow shock, stagnation point.

Article history:
Received: Jun. 1, 2022
Accepted: Jul. 28, 2022
Published: Sep. 01,2022

1. Introduction

Dust grains and embryonic ice materials are found on comets [1]. These materials have likely been produced and processed in the early phases of solar system development. The early solar nebula's chemical abundances have been deduced from the comet's frozen debris. Many water, carbon dioxide, and carbon monoxide molecules can be found in cometary ices [1]. Most comets in the inner solar system generate soft X-rays with a total emission power of (0.2–1.0 GW) in the (0.2–1.0 keV) range. In the 1990s, it was discovered that solar system objects undergo a process known as charge exchange, which results in X-ray emission. Cold gas is brought into touch with heated plasma or ionized cosmic rays, causing this reaction. It is the strong Coulomb force of ions that removes electrons from the cold gas. The electron then moves to an excited state of the ion and emits X-ray and UV lines as it descends to the ground state [2]. The emission spectra curves are the relation between photons account and the abundance of the material elements, where any spectrum has many peaks in the y-axis representing the energy or wavelength of these photons. There are so many curves at different ranges from radio to gamma waves of the object itself, but the range of our work is the X-ray band (Chandra analysis). Comets studied by the Chandra satellite reached the inner solar system after a long journey from the Oort cloud, which was observed by the satellite. Interacting energy of the solar wind with the atoms of the elements has many emission lines of every element from various atom levels. Photons account of elements spectrum lines have various peaks which means that the gas has different quantities of these elements per volume: thus, they

indicate elements abundance per cubic meter [3]. Analysis of X-ray emissions from comets is essential in determining the chemical makeup of the early solar system [4]. Even though comets are well-known as optically bright objects, [a recent study] has revealed that they are also X-ray luminous. C/ 1996 B2 (Hyakutake) was the first comet to show signs of X-ray emission: X-rays have already been detected in more than 30 other comets. Charge exchange between solar wind ions and neutral gases in the comet creates X-rays when a comet nears its perihelion. When solar X-rays collide with comet dust and ice particles, they scatter coherently and provide a large amount of energy to the overall emission intensity over 1 keV [5].

The purpose of this study is to investigate, analyze, and comprehend the many relationships between comets' dynamical and structural aspects. The comet system is described in detail using the relationships and properties listed above. The abundance, energy, number density and gas production rate were theoretically estimated for each element in a group of six comets. Bow shock, stagnation point and contact surface for five comets as a function of gas production rate were compared.

2. Data observations were from SAO image ds9 program

In this section the six comets that were observed by Chandra [6] will be discussed. On February 21, 2001, the McNaught-Hartley comet (C/1999T1) made its closest approach to the Earth at a distance of 1.2868 astronomical units (AU). It had a long period of cometary orbit with a perihelion distance of 1.1717 AU on declination 142000. The comet was found by McNaught in 1999 and is part of the Oort cloud [7]. 17P/Holmes comet was detected in an extraordinary state and in unusual geometries that were not seen before. The Jupiter-family comet Holmes began a massive outburst in October 2007 and continued until November 2007. Chandra's measurements show that 17P is the most gas-generating and furthest from the sun comet yet [8]. The Oort spike was the source of Sinding Spring (C/2013A1) [9]. The 103P/Hartley2 comet was separate from other short-period comets in the Kuiper belt, this one is an ecliptic comet. The comet 9P/Temple1 was classified as a Jupiter family comet having an orbital period under 20 years. The comet C/2001 Q4 (NEAT) has a retrograde orbit that is almost perpendicular. Its semi-major axis, perihelion, and aphelion are all unknown, as is its orbit [10].

3. Mathematical equations

Many characteristics of cometary gases are explained by mathematical equations, where each element's unique characteristic is described. The atoms of the elements that interact with the solar wind produce several emissions lines at various atom levels for each element. The spectrum of each comet depending on elements energy has been appeared in Fig.1.

3.1. The abundance of X-ray spectrum elements

The number of photons is a numerical representation of the total number of photons the source has emitted. Each gas component's photonic peak may be seen on the spectrum's curve. There is a direct correlation between atoms count and the peak number of photons. In other words, as the atoms count grows, so does the number of photons emitted [11]. When the number of photons increases as the number of atoms increases, the abundance also increases as seen in Fig.2. The ratio of any two peaks indicates the ratio of both these components' abundances, as in the following equation, a high peak denotes a high abundance [12]:

$$x_r = \frac{A_i}{A_c} \quad (1)$$

where x_r is the ratio of the element's relative abundance A_i to the carbon's relative abundance A_c. The observed carbon abundance x_C in the comet's gas must be known to calculate the abundance of all elements by multiplying Eq.(1) by the x_C value, to produce [13]:

$$x_i = \frac{A_i}{A_C} x_C \quad (2)$$

where x_i is the observed abundance of any element (i), and the total abundance of all elements is given by Eq. (3):

$$x_C = \frac{XA_C}{\sum_{i=1}^{N_i} A_i} \quad (3)$$

The limit $\sum_{i=1}^{N_i} A_i$ represents series limits, which are photons account of spectrum curve. The general formula of any elements' group that have known atomic masses m_i and their numbers N_i can be calculated from [14]:

$$\mathrm{X} = \frac{4.37512\, N_i}{[\sum_1^n m_i] - 23.4841 N_i} \quad (4)$$

Atomic mass (m_i) is given in the AMU unit, while the types of elements in each comet and its numbers have been illustrated in Table 1. The relation between the energy of each element with the atomic number has been shown in Fig.3.

3.2. Number density (n)

It has been discovered that it reproduces reported electron number densities at low activity and within a few tens of kilometers of the nucleus. In particular when plasma production through photoionization and electron impact ionization is taken into account. The number of photons equals the number of emitted atoms [15]:

$$\frac{n}{V} = (2 * 10^7\, k^{-3} m^{-3})\, T^3 \quad (5)$$

The number of atoms n(v) gives similar emitted photons from atoms which is a function of temperature. It is a constant value without effect the abundance; therefore, there is one variable only which is the abundance itself. Thus the equation must be as follow [4]:

$$\frac{n}{V} = \mathrm{X}\, (2 * 10^7\, k^{-3} m^{-3})\, T^3 \quad (6)$$

This relation is explained in Fig.4 by drawing the number density as a function of atomic number.

3.3. Gas production rate (Q)

Comets contain abundant amounts of organic and inorganic species. In addition to the inherent qualities of the comet, such as its size and its heliocentric distance, the overall gas production rate influences the activity of the comet and consequently, its size [16]. On the surface of the cometary nucleus, the rate of gas generation depends

on the radius of the nucleus and the velocity of gas outflow; the equation of this rate is as follows [17, 18]:

$$\mathbf{Q = n(r) * 4 \pi r^2 v} \qquad \mathbf{(7)}$$

The change in gas production rate with the atomic number can be seen in Fig.5.

3.4. Bow shock (R_B)

The bow shock is the first boundary the solar wind encounters as it approaches comets. The Rosetta spacecraft was able to observe the makeup of a bow shock by following the comet towards the Sun, through perihelion, and back outward again [19]. In the solar wind, cometary nuclei create ions that gyrate around field lines of the interplanetary magnetic fields when they are injected. Compared to the speed of the solar wind, the ionized particles' velocity is very low, hence they will only contribute mass to the plasma. As a result, the interaction between the comet's solar wind and its extra mass is dominant. Plasma flow near the comet will be re-distributed as the component velocities are swiftly established. The bow shock is created as the average molecular weight rises. The flow will be diverted around the comet as a result. The solar wind protons are thought to slow down as a result of this shock. The nucleus's bow shock can be computed by [20]:

$$\boldsymbol{R_B = \frac{G\, m_c\, \sigma\, (\gamma^2 - 1)}{4\, \pi\, V_c \rho_\Theta V_\Theta}} \qquad \mathbf{(8)}$$

where: $\boldsymbol{G}$ is the Gas production rate, $\boldsymbol{m_c}$ is constant molecular mass, $\boldsymbol{\sigma}$ is ionization rate, $\boldsymbol{V_c}$ =1 km.s^{-1} for the neutral gas, $\boldsymbol{\rho_\Theta}$ is the density and $\boldsymbol{V_\Theta}$ the velocity of the solar wind. When the overall gas production rate rises, the bow shock distance will rise in a linear fashion.

3.5. Stagnation point (R_S)

When the Mach number of the unperturbed solar wind is known, the stagnation pressures of the solar wind may be estimated using the dynamics equations of gas. Only at the location of the inner shock would the stagnation pressure be proper. However, there are no predictions for the thickness of an extended cometary ion layer based on a point source of cometary ions. A rough estimation of the standoff distance can be obtained by [21]:

$$\boldsymbol{R_s = \frac{G\, m_c\, \sigma}{4\, \pi\, \rho_w u_w^2}} \qquad \mathbf{(9)}$$

where: $\boldsymbol{\rho_w}$, $\boldsymbol{u_w}$ is the density and dynamic pressure respectively.

3.6. Contact surface (R_C)

Plasma will flow slowly between the bow shock and the nucleus in this region. Cometary ions' net pressure is equal to the solar wind's pressure at the magnetopause and stagnation of the solar wind in magneto- hydrodynamic models (MHD). There is no solar wind plasma or magnetic field beyond this surface. The standoff distance of the contact surfaces can be obtained using the following equation, [20]:

$$R_c = \frac{G\, m_c\, \sigma\, \Omega}{4\, \pi\, V_c \rho_\Theta V_\Theta} \qquad (10)$$

where: Ω is the influence of chemical processes like photodissociation. All the results of Eqs. (8, 9, and 10) change with the gas production rate proportional as illustrated in Fig.6.

4. Results and discussions

Using the Matlab program the resulted spectrum curve is in two dimensions, where the y-axis represents photons account that is delivered in satellite sensors and the x-axis is the energies from (1-10 keV). The line peaks indicate the energy levels of a certain element. Fig.1 shows the primary curve of many energy peaks which was recorded from the ds9 program.

4.1. Photons number

Fig.1 show that the photons number of each element depends on its energy. The elements in the comets can be known from their spectrums as observed from Chandra observatory in the X- ray band.

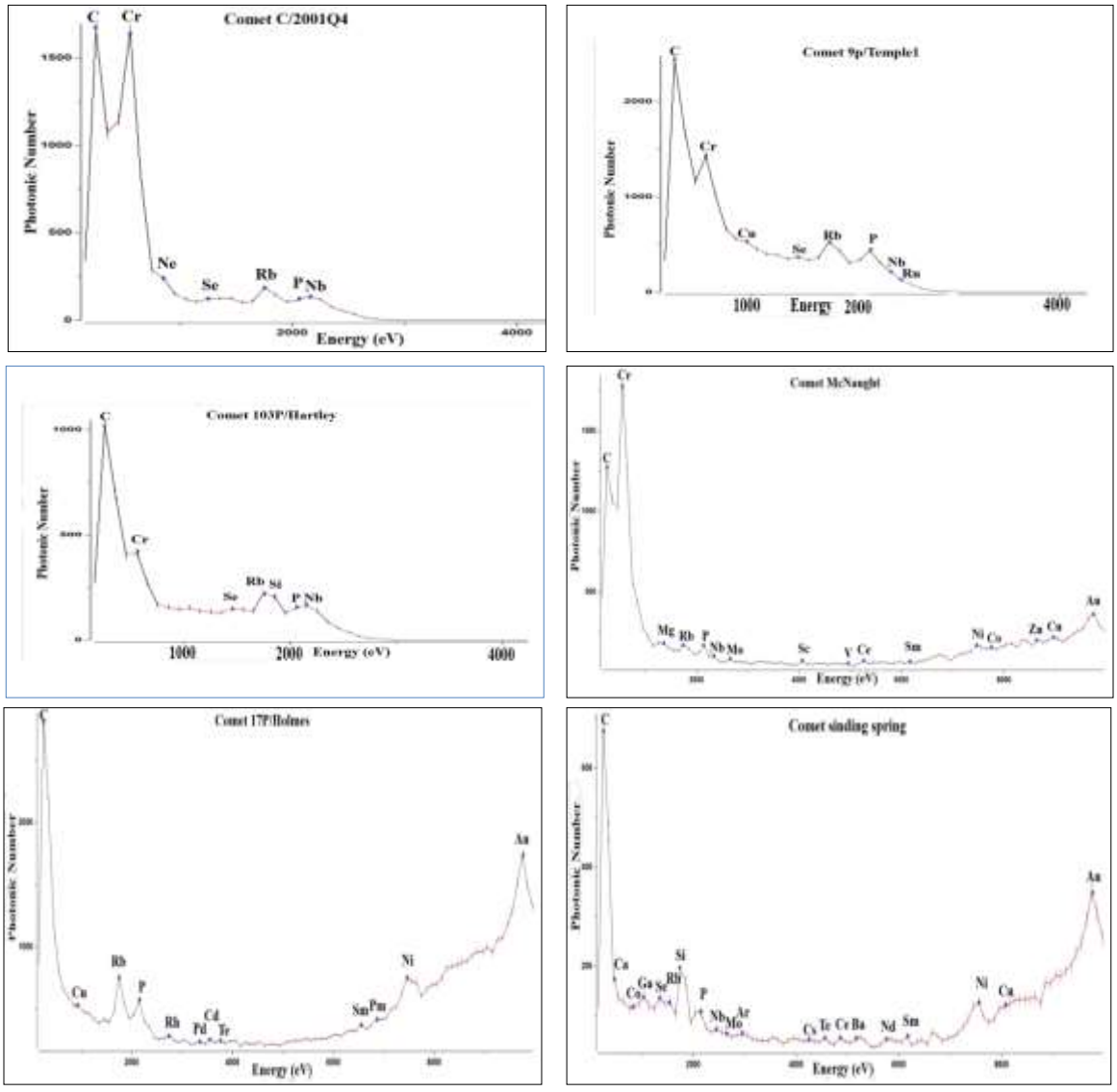

Figure 1: Photons number as a function of Energy.

4.2. Apparent abundance

Fig.2 shows symmetrical features for all the comets. The abundance decreases and increases with atomic number Carbon have the highest abundance.

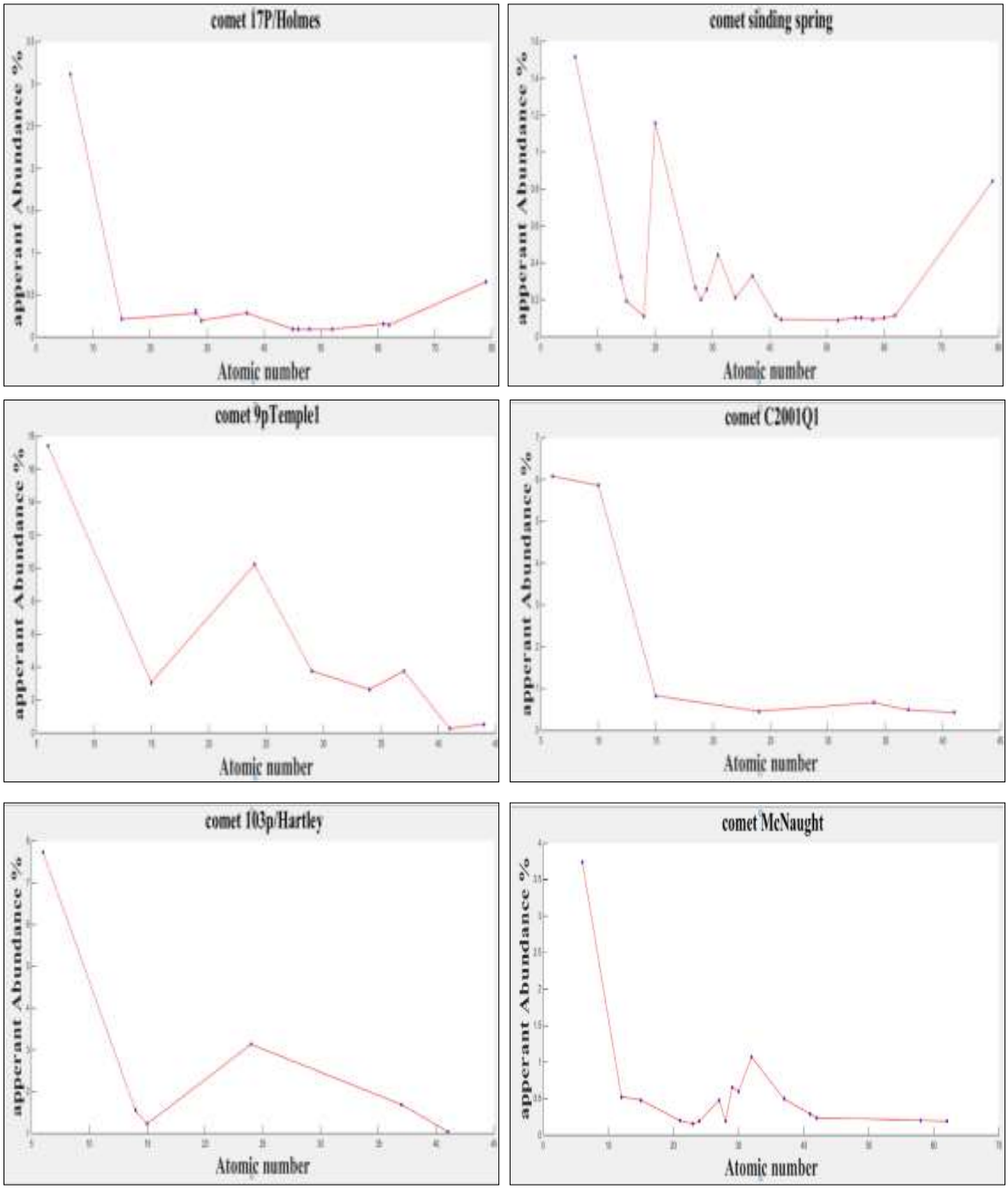

Figure 2: Six comets' apparent abundance by atomic number.

Table 1: Abundance of elements in the studied comets.

Comets	Elements	Number of elements
17P/Holmes	C- P- Ni- Cu- Rb- Rh-Pd- Cd- Te- Pm-Sm- Au	12
McNaught	C- Mg- P- Sc- V- Cr- Co- Ni- Cu- Zn- Au- Rb- Nb- Mo- Ce- Sm	16
Sinding spring	C- Si- P- Ar- N- Na- Ni- Cu- Ga- Au- Se-Rb- Nb- Mo- Te- Cs- Ba- Ce- Nd- Sm	20
C/2001Q4	C- Ne- P- Cr- Se- Rb- Nb	7
9P/Temple 1	C- P- Cr- Cu- Se- Rb-Nb- Ru	8
103P/ Hartley	C- Si- P-Se- Cr- Rb- Nb	7

4.3. Energy

The search has found two groups of elements in each comet with a particular arrangement style where: the elements with low atomic numbers tend to interact with solar wind particles at low energy, and the energy increases with high atomic numbers.

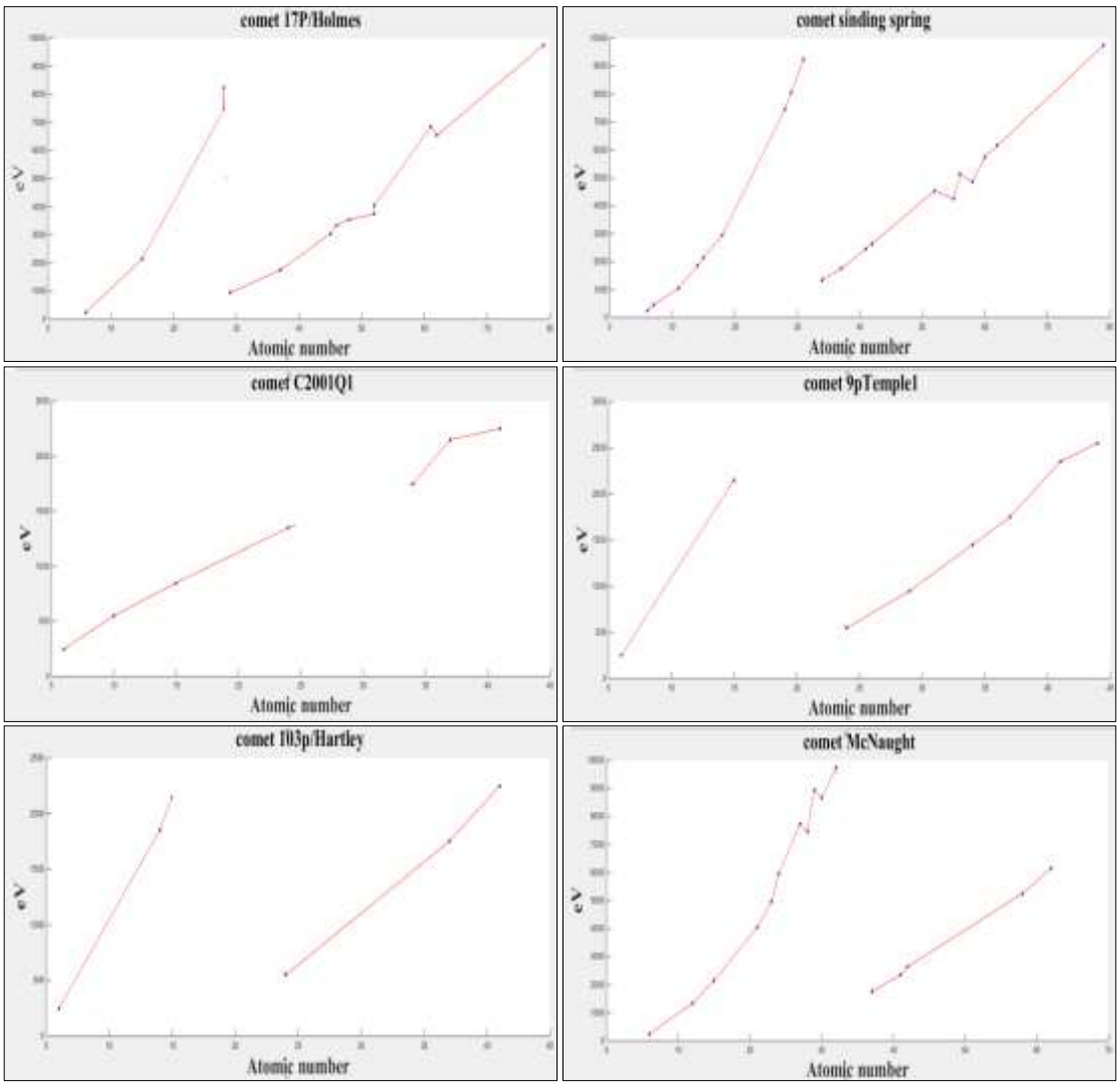

Figure 3: Energy versus comet' atomic number.

4.4. Number density

It has been demonstrated that the particle number density, which determines the ratio between photons and atomic number for each component, is important. The ratio of the population density to the gas production rate is direct.

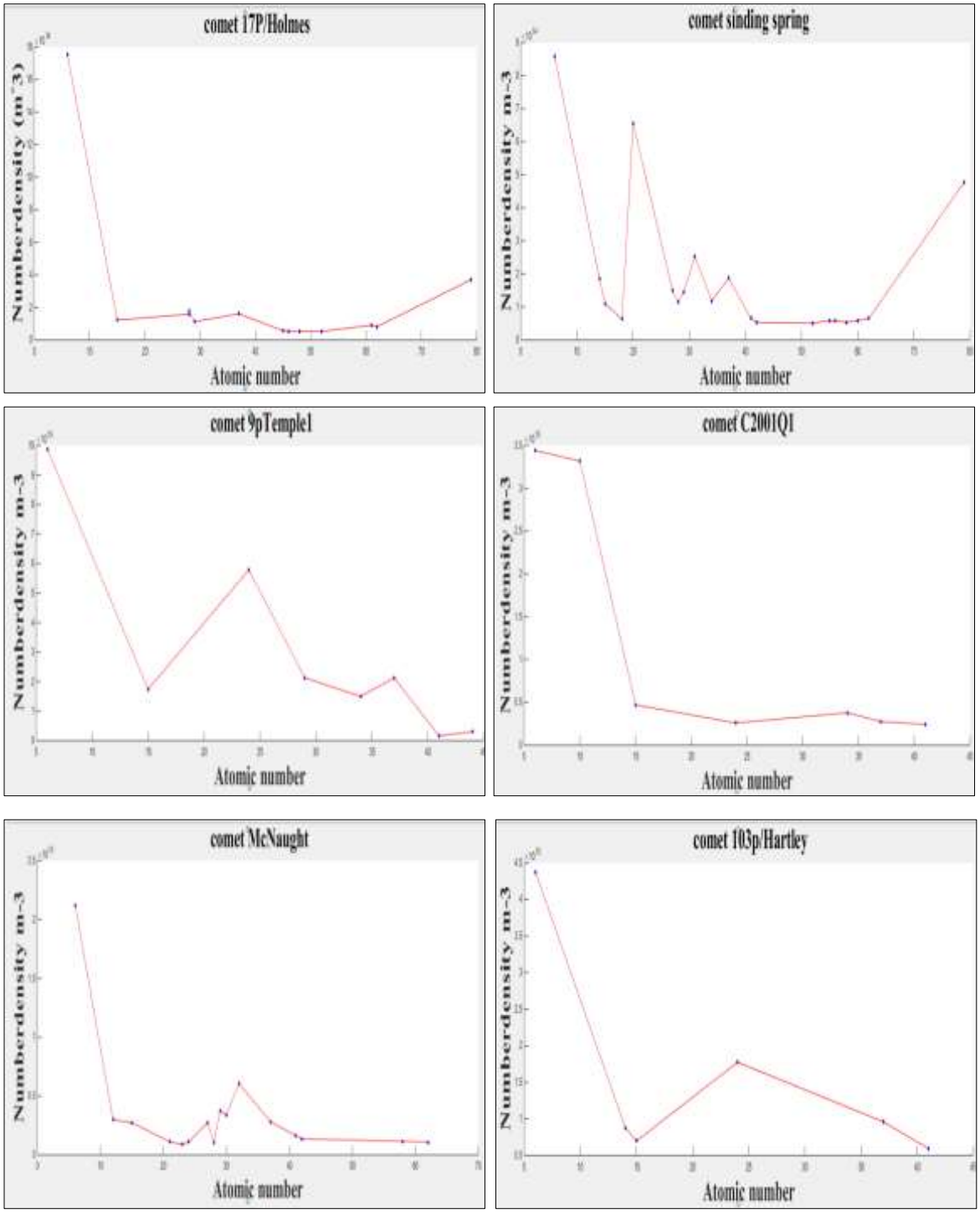

Figure 4: Comet number density versus atomic number.

4.5. Gas Production rate

Finally, fig.5 shows the gas production rate versus the atomic number that was calculated depending on the number density of each element in every comet. The general range of gas production rate is $(10^{27} - 10^{31})s^{-1}$, so our results are in the expected range.

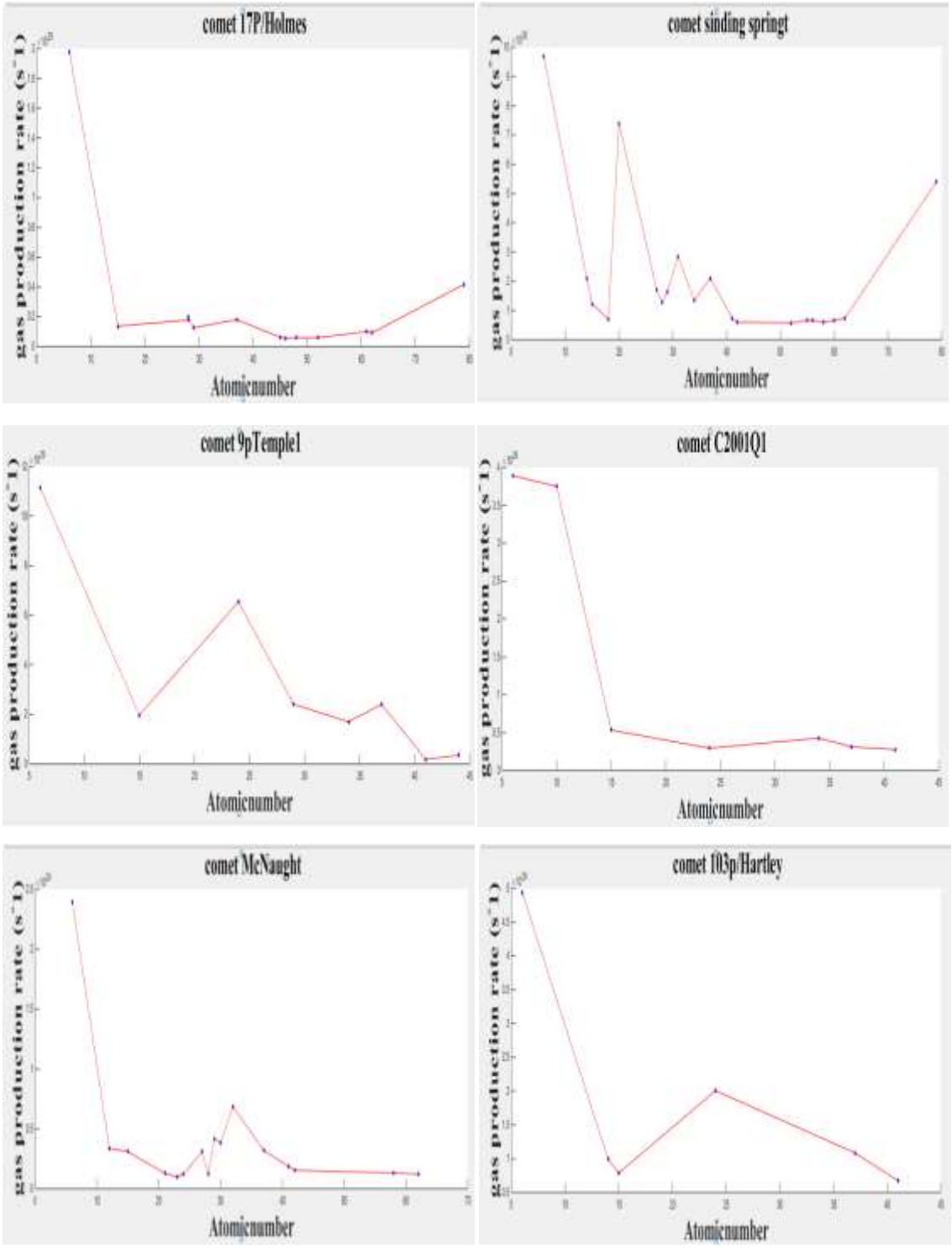

Figure 5: Gas production rate as a function of atomic number.

4.6. Stagnation point, contact surface and bow shock dependence on gas production rate

Comet features such as Bow shock Rb, stagnation Rs, and contact surface R_c are all affected by gas production rate (Q). A great deal of information about the comet's dynamics and structure is gleaned from this number. From here, some of the kinetic and structural characteristics of comets based on the amount of gas production were studied.

Stagnation point, contact surface, and bow shock all rise in tandem with the comet's gas production rate (Q). We demonstrated how cometary ions interact with the solar wind plasma and how this affects the (R_s, R_c, and R_b) by showing how the bow shock and contact surface form. According to several factors, such as the molecular weight and rate of emission of the comet's nucleus, changes in the bow shock's magnitude can be predicted. In both cases, the basic rule is based on the idea of energy conservation. Heavy molecular weights will ensure that the solar wind and cometary ions can exchange more energy. The same is expected to happen if gas output increases. This led to an increase in the bow shock distance. The relationships between Q and R_b, R_s and R_c thus represent changes in the system as a result of the comet's definition. As can be seen in Fig.6, the standoff distance Rs increases as Q increases.

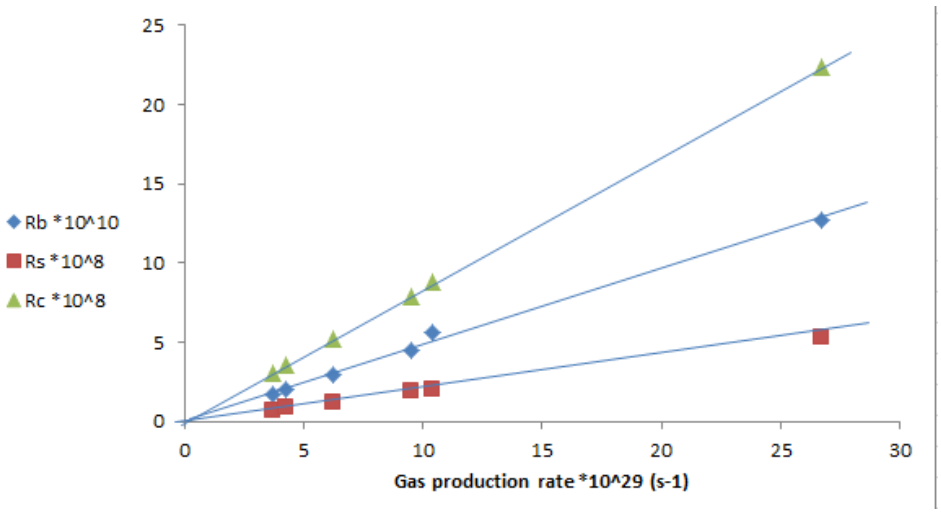

Figure 6: Bow shock R_b, stagnation R_s and contact surface R_c as a function of gas production rate Q of five comets.

5. Conclusion

The carbon element appears in all of the comets analyzed in this study: it has the highest rate of abundance based on X-ray examinations. It has been discovered that, in addition to carbon, two other elements, phosphorus and rhodium, exist in all comets analyzed. Three comets began in the Oort cloud: Mc Naught, Sinding spring, and C/2001Q4; three comets originated in the Kuiper belt: 17P/Holmes, 103P/Hartley, and 9P/Temple1. Heavy elements like gold could be discovered in three comets, two of which have high abundance, but the other one has a low abundance. In this study, the energy curves were separated into two groups: light elements with atomic numbers less than 30 AU and heavy elements with atomic numbers greater than 30 AU. This

research found that heavy elements are more abundant than light ones in the studied comets, except for comet Mc Naught, which has more light elements than heavy elements. The number density and gas production rate of comets with the same atomic number behaves similarly. The ratio and size of the bow shock, stagnation point, and contact surface were positively associated with the gas production rate of elements in the atmosphere of comets.

Acknowledgements

The authors are grateful to the department of Astronomy, College of Science, University of Baghdad all provided funding for the project.

Conflict of interest

Authors declare that they have no conflict of interest.

References

1. Ootsubo T., Kawakita H., Hamada S., Kobayashi H., Yamaguchi M., Usui f., Nakagawa T., Ueno M., Ishiguro M., Sekiguchi T., Jun-ichi W., Sakon I., Shimonishi T., and Onaka T., *AKARI near-infrared spectroscopic survey for CO_2 in 18 comets.* The Astrophysical Journal, 2012. **752**(15): pp. 1-12.
2. Ezoe Y., Ohashi T., and Mitsuda K., *High-resolution X-ray spectroscopy of astrophysical plasmas with X-ray microcalorimeters.* Reviews of Modern Plasma Physics, 2021. **5**(4): pp. 1-43.
3. Jalil M.I., Khalaf S.Z., and Abbas Q.A., *X-ray emission spectroscopy for the plasmas of 153P/Ikeya-Zhang and 46P/Wirtanen comets.* Global Scientific Journal, 2021. **9**(1): pp. 1952-1959
4. Xing Z., Bodewits D., Noonan J., and Michele T. B., *Water production rates and activity of interstellar comet 2I/Borisov.* The Astrophysical Journal Letters, 2020. **893**(2): pp.1-10.
5. Abbas K.H., Khalaf S.Z., and Selman A.A., *Calculation of the interactions between solar wind particles and cometary ion tail.* Science International (Lahore), 2018. **30**(5): pp. 729-736.
6. https://chandra.harvard.edu/learn_solar.html.
7. Lara L.M., Licandro J., and Tozzi G., *Dust in comet McNaught-Hartley (C/1999 T1) from Jan. 25 to Feb. 04, 2001: IR and optical CCD imaging.* Astronomy & Astrophysics, 2003. **404**(1): pp. 373-378.
8. Christian D. J., Bodewits D., Lisse C. M., Dennerl K., Wolk S. J., Hsieh H., Zurbuchen T. H., and Zhao L., *Chandra observations of comets 8p/Tuttle and 17p/Holmes during solar minimum.* The Astrophysical Journal Supplement Series, 2010. **187**(2): pp. 447-459.
9. Wajer P. and Królikowska M., Comet C/2013 A1 siding spring. How treatment of data and NG effects can change our predictions about close encounters with Mars. ASTEROIDS, COMETS, METEORS 2014 (ACM'2014) conference, 2014: pp. 1-5, Special Issue of Planetary and Space Science.
10. Mumma M. J., Bonev B. P., Villanueva G. L., Paganini L., DiSanti M. A., Gibb E. L., Keane J. V., Meech K. J., Blake G. A., Ellis R. S., Lippi M., Boehnhardt H., Magee-Saucer K., *Temporal and spatial aspects of gas release during the 2010 apparition of comet 103P/Hartley 2.* The Astrophysical Journal Letters, 2011. **734**(1): pp.1-6.
11. Perryman M., *The exoplanet handbook.*, 2nd Ed, 2018: Cambridge University Press.

12. Khalaf S.Z. and Abrahim K., *Expansion velocities of elementary gas in comet Panstarrs above 30000 km from nucleus.* Iraqi Journal of Science, 2020. **61**(12): pp. 3417-3433.
13. Yamamoto T., *Chemical composition of cometary ice and grain, and origin of comets*. *Symposium-International Astronomical Union*. 1987. Cambridge University Press.
14. Abood K.I., *Structure and nucleus characteristic of the ion cometary tail.* PhD, University of Baghdad, College of Science, Astronomy and Space Department, 2020.
15. Vigren E., Edberg N. J. T., Eriksson A. I., Galand M., Henri P., Johansson F. L., Odelstad E., Rubin M., Vallières X., *The evolution of the electron number density in the coma of comet 67P at the location of rosetta from 2015 November through 2016 March.* The Astrophysical Journal, 2019. **881**(1):pp.1-5.
16. Bhardwaj A., *On the solar EUV deposition in the inner comae of comets with large gas production rates.* Geophysical research letters, 2003. **30**(24): pp.1-5.
17. Bleeker J.A., Geiss J., and Huber M.C., *The century of space science*. 1st Ed, 2001. Springer.
18. Läuter M.,Tobias K., Martin R., Kathrin A., *The gas production of 14 species from comet 67P/Churyumov–Gerasimenko based on DFMS/COPS data from 2014 to 2016.* Monthly Notices of the Royal Astronomical Society, 2020. **498**(3): pp. 3995-4004.
19. Gunell H., Goetz C., Wedlund C.S., Lindkvist J., Hamrin M., Nilsson H., Llera K., Eriksson A., Holmström M., *The infant bow shock: a new frontier at a weak activity comet.* Astronomy & Astrophysics, 2018. **619**: pp.1-5.
20. Khalaf S.Z., Selman A.A., and Ali H.S., *Study of comets composition and structure.* Al-Nahrain Journal of Science, 2008. **11**(3): pp. 80-88.
21. Buti B., *Cometary and solar plasma physics.* Cometary and Solar Plasma Physics, World Scientific,1988.

التحليل الطيفي لانبعاث الأشعة السينية بالقرب من حزام الكويكبات في الغلاف الجوي للمذنبات

رشا سهيل نجم[1]، سلمان زيدان خلف[1]، خليل إبراهيم عبود[1]
[1]قسم الفلك والفضاء، كلية العلوم، جامعة بغداد، بغداد، العراق

الخلاصة

ان البحث الحالي يركز على طبيعة و خصائص التفاعلات بين الرياح الشمسية مع المذنب الذي ينتج أنواعً طيفية مختلفة في المذنبات القريبة من حزام الكويكبات و قد تمت دراسة الأشعة السينية الناتجة عن تبادل الشحنات بين الرياح الشمسية و الغلاف لمحيط بالمذنب. يمكن الكشف عن الكثير من المعلومات حول تكوين المذنبات من أطيافها وقد ركز هذا البحث على وفرة العناصر في ستة مذنبات مختلفة وهي:

17P/Holmes, C/1999T1, C/2013A1, 9p/Temple1, 103p/Hartley2, C/2001Q4 (NEAT)

تمثل الحسابات التي تم إجراؤها في هذا العمل تحليل وتفسير السمات المختلفة للمذنب، مثل معدل إنتاج الغاز، واعتماد الأخير على تكوين الغلاف الجوي للمذنب (الغيمة). تم دراسة الصدمة المتمثلة على شكل قوس، وسطح التلامس، ومسافات الركود مع معدل إنتاج الغاز لعدة أنواع من المذنبات التي تغطي الأنواع الخطية وغير الخطية. كذلك تم الحصول على نتائج مهمة تشير إلى التفاعلات الفيزيائية المختلفة بين أيونات المذنبات والرياح الشمسية. علاوة على ذلك، تم تحليل ودراسة العلاقة المهمة بين متوسط الوزن الجزيئي ومعدل إنتاج الغاز في هذا البحث، ولخصت أنه مع زيادة معدل إنتاج الغاز سينخفض متوسط الوزن الجزيئي بشكل كبير وتم إعطاء مناقشة مفصلة لهذه العلاقات الفريد.